



Article

# Synthesis and Characterization of New Tetradentate N<sub>2</sub>O<sub>2</sub>-Based Schiff's Base Cu (II) Complexes for Dye Photodegradation

Rohini Vallavoju<sup>1</sup>, Ranjith Kore<sup>1</sup>, Radhika Parikirala<sup>1</sup>, Mahesh Subburu<sup>2</sup>, Ramesh Gade<sup>2</sup>, Vipin Kumar<sup>3</sup> ,  
Matta Raghavender<sup>1</sup>, Prabhakar Chetti<sup>3,\*</sup>  and Someshwar Pola<sup>1,\*</sup>

<sup>1</sup> Department of Chemistry, Osmania University, Hyderabad 500007, India

<sup>2</sup> Department of Humanities & Sciences, Yardhaman College of Engineering, Hyderabad 500007, India

<sup>3</sup> Department of Chemistry, National Institute of Technology, Kurukshetra 136119, India

\* Correspondence: chetti@nitkkr.ac.in (P.C.); somesh.pola@gmail.com (S.P.)

**Abstract:** We have reported tetradentate ligands (salophen) coordinated with N and O atoms that led to the Cu (II) complexes. These Cu (II) complexes (C-1 and C-2) were firstly established by using elemental analysis and confirmed by mass spectra. At the same time, the characterization of C-1 and C-2 complexes is performed by using several spectroscopic methods and morphological analysis. The bandgap values of the C-1 and C-2 complexes are evaluated with UV-vis DRS spectra. The PL spectral data and photocurrent curves clearly indicated the small recombination rate of the hole–electron pair. The synthesized C-1 and C-2 complexes' photocatalytic properties were examined for the degradation of cationic dyes such as methylene blue (MB  $\lambda_{\text{max.}} = 654$  nm) and methyl violet (MV  $\lambda_{\text{max.}} = 590$  nm) below visible-light action. The C-2 complex is more active than the C-1 complex because of its high photostability, small band-gap energy, and low recombination rate for hole–electron pair separation, and improved visible-light character, which encourages the generation of hydroxyl radical species throughout the photodegradation process. Scavenger probes were used to identify the dynamic species for the photodegradation of dyes, and a mechanism investigation was established.

**Keywords:** Cu (II) complexes; photocatalysis; surface area; rate of recombination; methyl violet dye



**Citation:** Vallavoju, R.; Kore, R.; Parikirala, R.; Subburu, M.; Gade, R.; Kumar, V.; Raghavender, M.; Chetti, P.; Pola, S. Synthesis and Characterization of New Tetradentate N<sub>2</sub>O<sub>2</sub>-Based Schiff's Base Cu (II) Complexes for Dye Photodegradation. *Photochem* **2023**, *3*, 274–287. <https://doi.org/10.3390/photochem3020016>

Academic Editors: Rui Fausto, Marcelo Guzman and Vincenzo Vaiano

Received: 26 March 2023

Revised: 27 April 2023

Accepted: 28 April 2023

Published: 11 May 2023



**Copyright:** © 2023 by the authors. Licensee MDPI, Basel, Switzerland. This article is an open access article distributed under the terms and conditions of the Creative Commons Attribution (CC BY) license (<https://creativecommons.org/licenses/by/4.0/>).

## 1. Introduction

The use of Schiff base ligands in coordination chemistry has been extensively studied, particularly those with tetradentate ligands containing nitrogen and oxygen donor atoms [1–5]. Metal (II) complexes of these ligands have shown promising catalytic activity in oxidative catalysis [6] and deoxygenation [7] reactions. Cu (II) Schiff base complexes, in particular, have received interest for their potential catalytic activity (conventional or photocatalytic) in the oxidation of organic substrates [8,9]. The use of Schiff base ligands derived from 2-hydroxy-1-naphthaldehyde and aryl-1,2-diamines in the synthesis of M(II) complexes has been extensively studied [10–12]. Among these, Cu (II) Schiff base complexes have been reported to exhibit various catalytic activities [13,14]. However, despite the large number of metal–Schiff base complexes available, Cu (II) Schiff base complexes are relatively less studied for their photocatalytic applications in organic transformations. The recent study on the piezo-photomineralization of MR and RhB cationic dyes using Cu (II) Schiff base complexes obtained from 4-chlorobenzene-1,2-diamine or 4-fluorobenzene-1,2-diamine with 2-hydroxy-1-naphthaldehyde is of great significance. The study can provide insights into the potential of Cu (II) Schiff base complexes as photocatalyst<sup>3</sup> in the degradation of organic pollutants [15–17].

Under visible-light irradiation, mono- and bimetallic complexes have been used to photodegrade organic pollutants [18]. Photooxidation of aromatic hydrocarbons and methylstyrenes have also been accomplished using Ru (II) and Zn (II) complexes with

Schiff base ligands [19]. Other studies have investigated the potential of Pd (II) Schiff base complexes for the synthesis of fused heterocyclic aromatic hydrocarbons and the activation of allylic C-H bonds and Ag-doped Pd (II) complexes under visible-light irradiation for the degradation of dyes [20,21]. Zn (II) complexes have also been investigated for their possible use in the photooxidation of 2,2'-(Ethyne-1,2-diyl) dianilines [22], the photodecomposition of organic dye pollutants [23], and the piezo-photomineralization of dyes and industrial waste [24]. More recently, Ti (IV) complexes obtained using salophen-based ligands have been explored for their potential piezo-photocatalytic degradation of methyl red and rhodamine B dyes [25].

In this study, the reactions of tetradentate Schiff base ligands obtained from 4-chlorobenzene-1,2-diamine or 4-fluorobenzene-1,2-diamine with 2-hydroxy-1-naphthaldehyde and Cu<sup>2+</sup> ions were investigated for their potential use in the photomineralization of MR and MV cationic dyes under visible-light treatment. The structures of ligands L-1 and L-2, and respective complexes C-1 and C-2 are given in Figure 1.

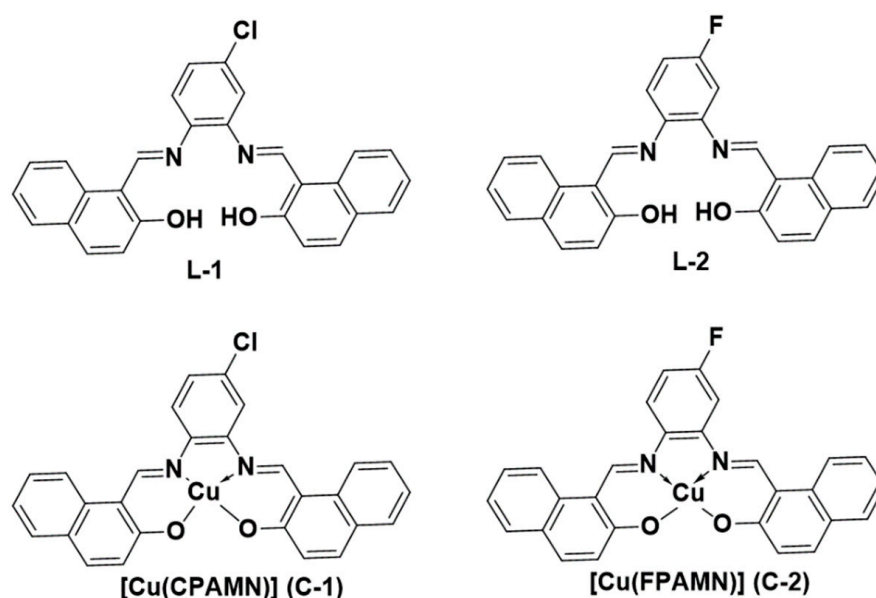


**Figure 1.** Structures of Schiff's base ligands and new Cu(II) complexes.

## 2. Materials and Methods

All the experimental processes for preparation of ligands were performed by following earlier methods [23]. The detailed experimental methods and characterization techniques for the analysis of Cu (II) complexes are shown in the Supplemental Materials. The carefully purified and dried Cu (II) complexes C-1 and C-2 were analyzed using elemental mass spectra, XPS, TGA, FTIR, FESEM, UV-visible emission, ESR, and photocurrent measurements.

### *Experimental Procedure for Photomineralization of Dye Pollutants*

The photocatalyst (30 mg) was placed into 80 mL dye pollutant solution ( $5 \times 10^{-4}$  M) in a 100 mL quartz glass cylindrical photoreactor. The mineralization of MR and MV cationic dyes was kept in the presence of visible light (300 Watts tungsten light with photon flux  $8.02 \times 10^{13}$  Einstein/s and wavelength 380–780 nm), as found by utilizing the chemical actinometric method with Reinecke salt [18] for 30 min. The adsorption–desorption equilibrium technique for the specific dye was attained in the absence of light for 10 min; the light was then permitted to fall on the reaction dye solution. Once the light was turned on, then a sample was taken every 5 min for UV-visible spectroscopic analysis. To verify the reusability of the catalyst, C-1/C-2 was separated by the centrifugal method, used again for the degradation of the dye, and its concentration studied using a UV-visible spectrophotometer at dye  $\lambda_{\text{max}}$ .

### 3. Results and Discussion

Molar conductivity experiments were used to determine if the new Cu (II) complexes were ionic or covalent. The conductivity of both C-1 and C-2 complexes was measured with the  $10^{-3}$  M concentrations and showed the values  $12.07$  and  $9.17 \text{ ohm}^{-1} \text{ mol}^{-1} \text{ cm}^2$ , respectively. These values indicated that both the complexes are covalent and nonelectrolytic in nature (Table S1) [25]. Further, after 72 hours, the complexes were reexamined for molar conductance and exhibited the same conductance. Hence, the Cu (II) complexes are highly stable as  $\text{Cu}^{2+}$  ions are strongly complexed with the salophen ligands. The elemental and physicochemical data for the C-1 and C-2 complexes are depicted in Table S1. The analytical data show that various elements such as Cu, Cl/F, N, C, and H agree with the theoretical data, which are empirically formulated as C-1 and C-2 complexes. The MALDI mass spectral data for complexes C-1 and C-2 coincide with the exact molecular weight and are outlined in Figures S1 and S2, respectively. The Cu (II) complexes spectra show that the  $m/z$  values of 511.1475, and 495.1571 are in agreement with the molecular ions of C-1 and C-2, respectively (Figures S1 and S2) [24].

X-ray photoelectron spectroscopy (XPS) can be a useful tool for analyzing Cu (II) complexes with nitrogen and oxygen donors. XPS can provide information about the chemical composition and electronic state of the elements in the sample. When performing XPS analysis, the sample is bombarded with X-rays, which cause the emission of electrons from the surface of the sample. The energies of the emitted electrons are then measured to determine the binding energy of each element in the sample. By analyzing the binding energies of the Cu, nitrogen, and oxygen atoms in the complex, information can be obtained about the chemical bonding in the sample. In Cu (II) complexes with nitrogen and oxygen donors, the Cu atom is typically coordinated to one or more nitrogen or oxygen atoms, forming a complex with specific coordination geometry. The XPS spectra of these complexes show peaks corresponding to the Cu 2p, nitrogen 1s, and oxygen 1s electron orbitals. The positions and intensities of these peaks can be used to determine the electronic state of the Cu atom and the chemical environment of the nitrogen and oxygen atoms.

The Cu 2p XPS peak for a Cu (II) complex with Cl-substituted Schiff's base ligand shifted to a slightly higher binding energy compared to the peak for a complex with a nonsubstituted Schiff's base ligand. The nitrogen 1s and oxygen 1s peaks can also provide information about the bonding between the ligand and Cu atom, and any changes in the electron density around the ligand due to the presence of the Cl atom, as shown in Figure 2. Similarly, the Cu 2p XPS peak for a Cu (II) complex with an F-substituted Schiff's base ligand shifted to a slightly lower binding energy compared to the peak for a complex with a nonsubstituted Schiff's base ligand. The nitrogen 1s and oxygen 1s peaks can also provide information about the bonding between the ligand and Cu atom, and any changes in the electron density around the ligand due to the presence of the F atom, which is shown in Figure 3; details of analysis are mentioned below.

The XPS spectrum of the C-1 complex displays peaks at 965.09, 955.76, 945.9, and 935.99 eV for the  $2p_{1/2}$  and  $2p_{3/2}$  states of Cu of Cu-O and Cu-N bonds, respectively [26,27]. The remaining peaks, such as 203.24 eV for Cl (2p); 534.09 and 531.91 eV for O (1s); and 399.13 and 400.33 eV for Cu-N and Ar-C=N-Ar N (1s) states [21,28], are also displayed. In the case of the C-2 complex, 965.13, 955.55, 945.09 and 935.71 eV are indicated for the Cu-N and Cu-O ( $2p_{1/2}$  and  $2p_{3/2}$ ) bonds. Additionally, 688.01 for F (1s), 533.52 and 531.81 eV for O (1s), and 399.24 and 400.48 eV N (1s) peaks are observed in C-2; three different peaks are present in both the C-1 and C-2 complexes for C (1s), such as 285.27, 285.55, and 285.99 eV for C-Cl, C-OAr, and -C=N-, respectively, for C-1; and for the C-2 complex, 284.80, 285.35, and 286.31 eV for C-F, C-OAr and -C=N-, respectively, as revealed in Figures 2 and 3.

To know the thermal stability and thermal decomposition path for both Cu (II) complexes, thermogravimetric (TG) analysis of both complexes was investigated under a nitrogen atmosphere from 50 to 750 °C with an evaporating rate of  $10 \text{ }^\circ\text{C min}^{-1}$ . The TGA of the C-1 complex decomposed at 385 °C, whereas the C-2 complex started at 395 °C. Both the Cu (II) complexes were decomposed in a single step, which designated that the ratio of

ligand to metal is equal (1:1) [25] and revealed the conforming disintegration thermogram in Figure 4. The experimental TG plots display that C-1 and C-2 complexes decompose ligands in the solo stage with a weightiness loss of 84.38% (calcd. 84.56%) between 385 and 500 °C [25]. The TG curvature displays a mesa between 350–500 °C, and then there is no further disintegration up to 750 °C. The values obtained agree, indicating that the end material is pure CuO, which is confirmed by XPS and p-XRD data, as shown in Figure 5 and Figure S3 for the respective complex's residual substance.

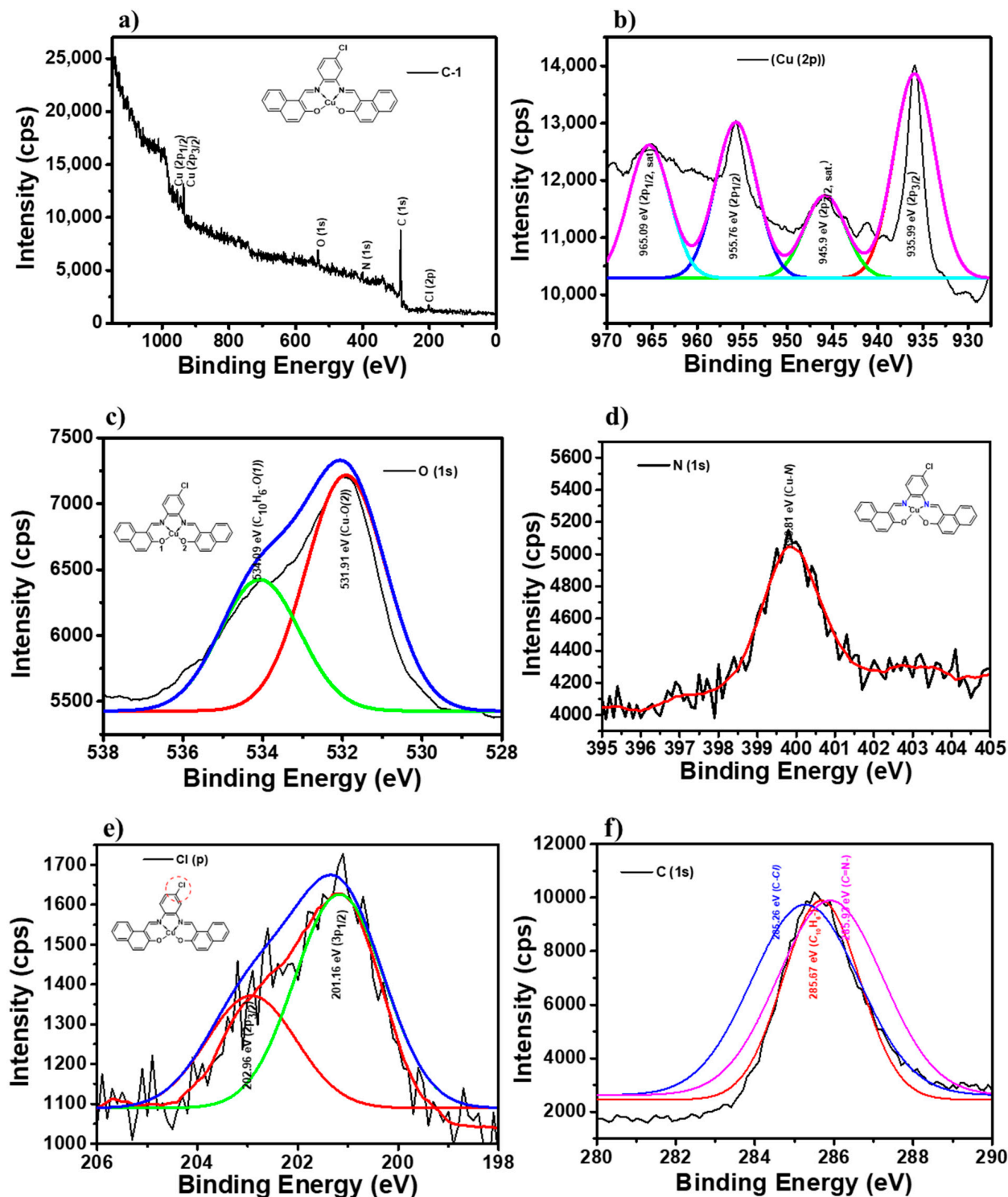


**Figure 2.** XPS spectra: (a) overall survey spectra; (b) Cu (2p) spectra; (c) O (1s) spectra; (d) N (1s) spectra; (e) Cl (2p) spectra; and (f) C (1s) spectra of the C-1 complex.

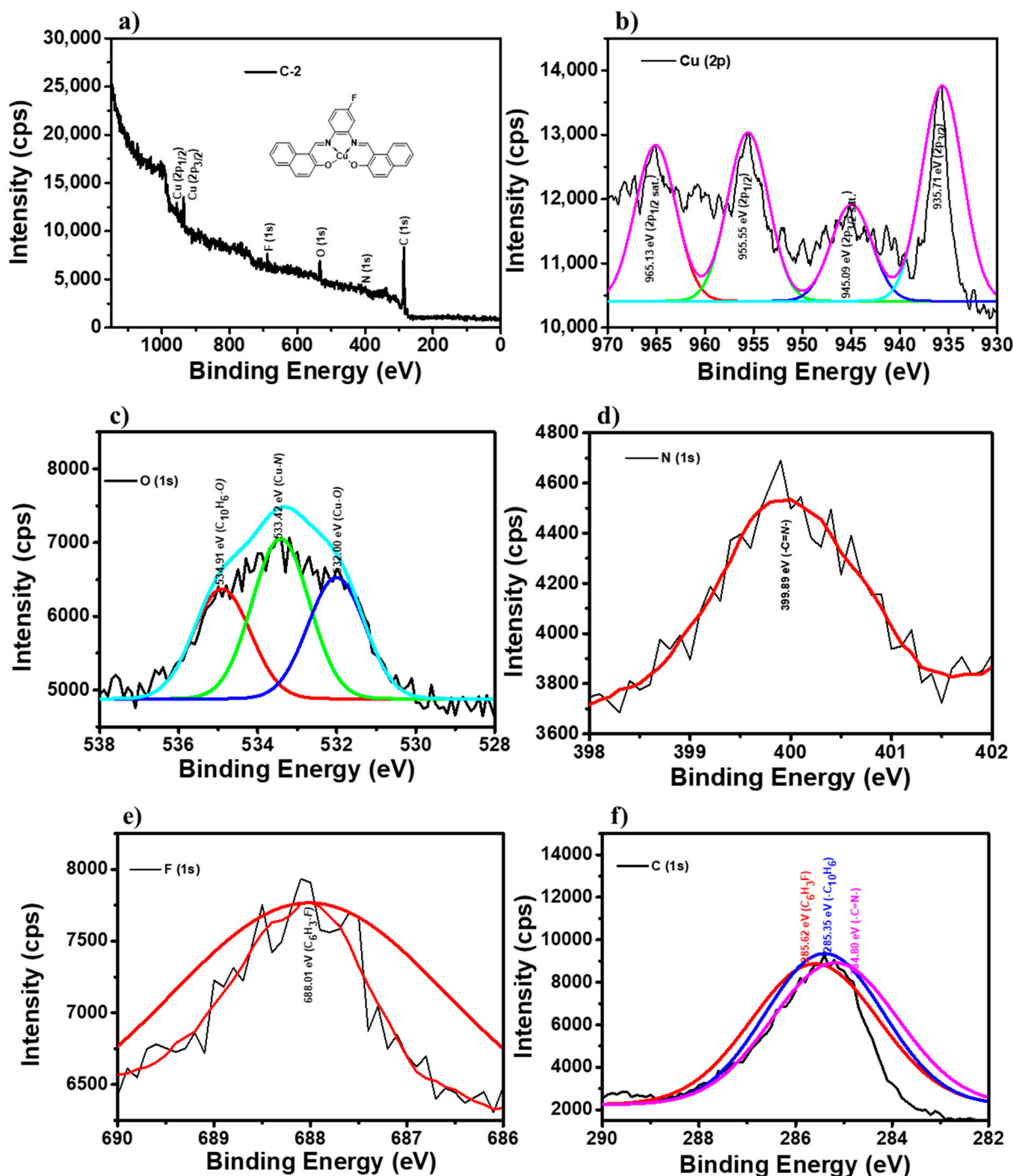


**Figure 3.** XPS spectra: (a) overall survey spectra; (b) Cu (2p) spectra; (c) O (1s) spectra; (d) N (1s) spectra; (e) F (1s) spectra; and (f) C (1s) spectra of the C-2 complex.

FTIR was used to confirm the bonding vibrational modes of all the ligands and Cu (II) complexes. The weak and strong peaks noticed at  $1578$  and  $1452\text{ cm}^{-1}$  in the spectrum of the ligand L-1 is known to be the vibrational stretching modes of the imine ( $-\text{C}=\text{N}-$ ) group [24]. In both the Cu (II) complexes, vanishing of the phenolic groups as correlated to ligand

spectra and azomethine group peaks are shifted to the higher wavenumber side, which designates the complexation of the azomethine group. The two novel stretching modes in the FTIR spectra of C-1 and C-2 complexes, one around 403 and 406  $\text{cm}^{-1}$  and the other around 504 and 502  $\text{cm}^{-1}$ , have been identified as  $\nu(\text{Cu-N})$  and  $\nu(\text{Cu-O})$ , respectively. The vibrational modes shown in the FTIR spectra of Cu (II) complexes signify that the  $\text{Cu}^{2+}$  ions are complexed with L-1/L-2 via two  $-\text{C}=\text{N}$ -functional and two  $\text{Ar-OH}$  sets. The illustrative FTIR spectra of Cu-complexes, C-1 and C-2, are revealed in Figures S4 and S5, respectively.

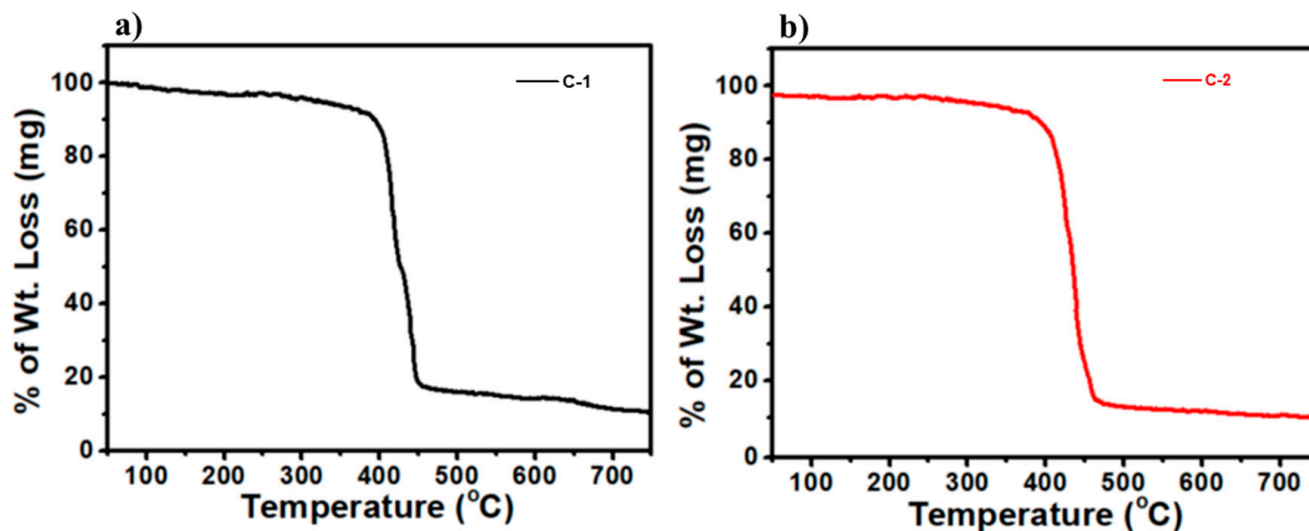


Figure 4. Thermograms of (a) C-1 and (b) C-2 complexes.

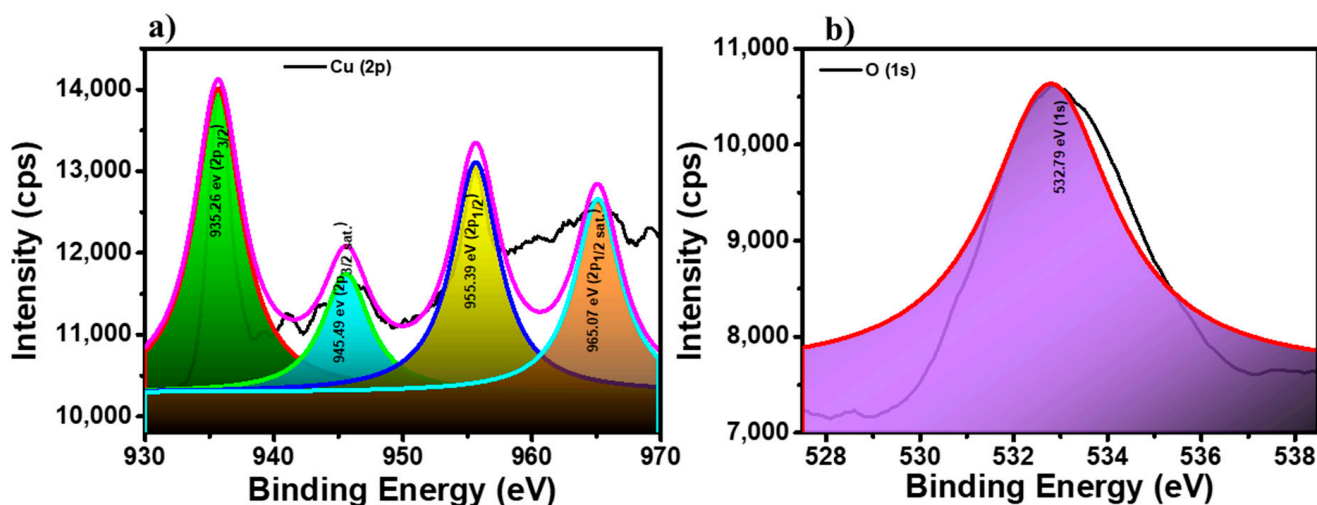


Figure 5. XPS spectra of CuO residue (a) Cu (2p) and (b) O (1s) obtained from TG analysis.

The electron spin resonance (ESR) spectra of the Cu (II) complexes are presented in Figure 6a,b. The spectra of the two complexes are anisotropic in nature, and each one exhibits three peaks. The  $g_{\parallel}$  and  $g_{\perp}$  were calculated from the spectra (Table 1). ESR spectra of the complexes provide an excellent basis for distinguishing the unpaired electron as being present in either the ground state  $dx^2 - y^2$  or the ground state  $dz^2$ . Thus, using the equation  $(g_2 - g_1)/(g_3 - g_2)$ , if the value of R is greater than one, the electron is present in  $dz^2$ , and if the value is less than one, the electron is present in  $dx^2 - y^2$ . In the case of C-1, the R value is 0.263 and was found that  $g_{\parallel} > g_{\perp} > 2$  for both the complexes, indicating that the unpaired electron is present predominantly in the  $dx^2 - y^2$  orbital of the Cu (II) ion. This indicates that these complexes are monomeric in nature, and that there are no metal-metal interactions and exchange couplings [29].

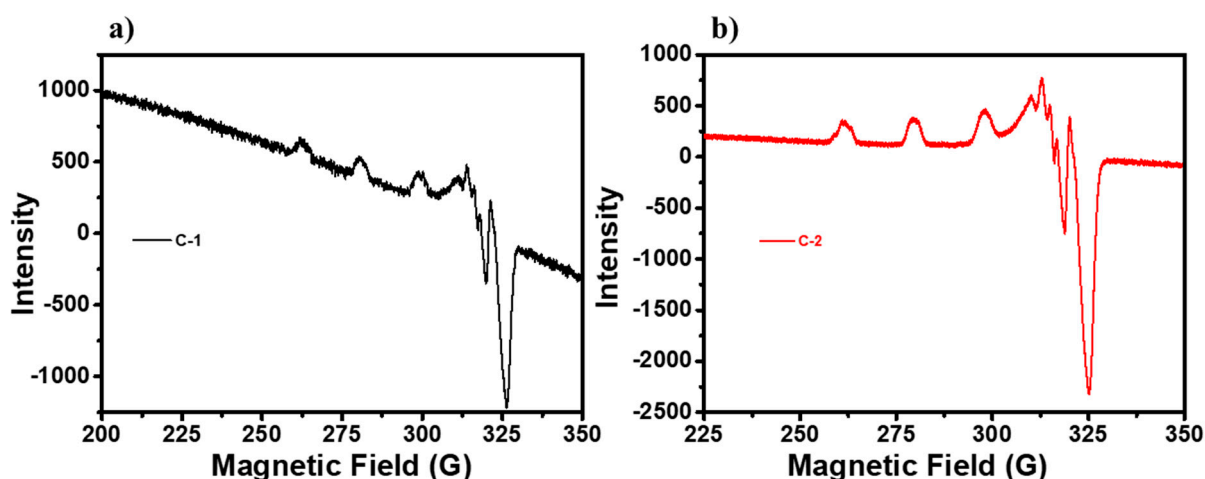


Figure 6. ESR spectra of (a) C-1 and (b) C-2 complexes.

Table 1. ESR parameters of Cu (II) complexes.

Complex	$g_{  }$	$g_{\perp}$	$g_{ave}$
C-1	2.36	2.088	2.224
C-2	2.38	2.099	2.239

### 3.1. Absorption and Emission Studies

The UV-visible spectra of the Schiff base ligands L-1 and L-2 were analyzed in DMSO and showed absorption bands between 330 and 425 nm [24,30]. The onset bands of the Schiff bases are at 504 and 512 nm for L-1 and L-2, respectively, indicating that the bandgap of the Schiff bases falls between 2.43 and 2.42 eV. Upon complexation with Cu(II) ions, the absorption bands of the Cu(II)-complex shifted to the higher wavelength side (Figure 7) [28–30], indicating the occurrence of ligand–metal charge transfer and the strong interaction of lone-pair electrons of donor N-atoms with  $\text{Cu}^{2+}$  ions. The bandgap energies of the Cu(II) complexes were found to be lower than those of the pure Schiff base compounds, as shown in Table 2. This suggests that complexation with Cu(II) ions could enhance the absorption and utilization of visible light by the Schiff base ligands for photocatalytic applications.

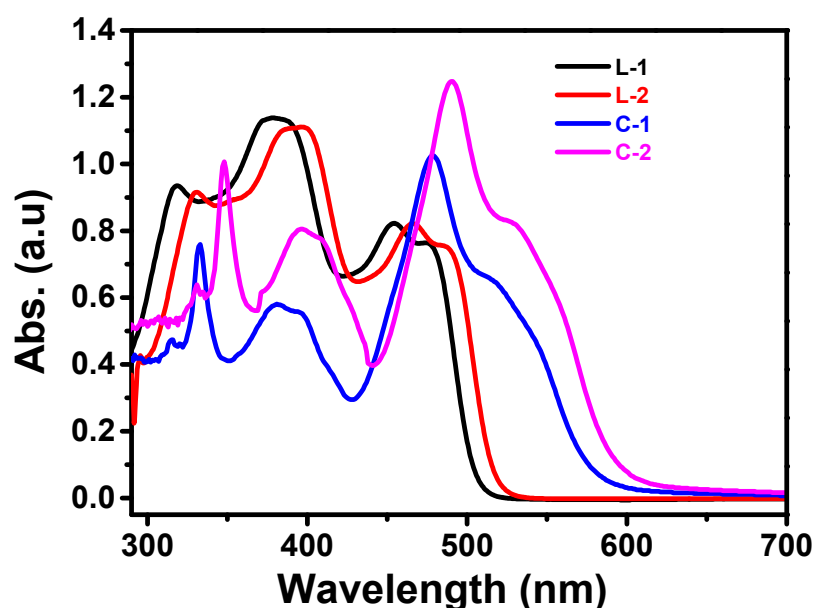


Figure 7. UV-vis spectra of the L-1 and L-2 ligands and the C-1 and C-2 complexes.

**Table 2.** Experimental  $\lambda_{\text{onset}}$  (nm), bandgap energies (in eV), and surface area of Cu (II) complexes.

Name	$\lambda_{\text{onset}}$ (nm)	Bandgap Energy (eV)	Surface Area (m <sup>2</sup> /g)
L-1	504	2.46	5.8
L-2	512	2.42	6.9
C-1	584	2.12	45.6
C-2	599	2.07	62.3

Surface areas of the ligands L-1 and L-2 were far smaller than Cu (II) complexes C-1 and C-2, as given in Table 2 [31].

DFT and TD-DFT calculations were also performed to gain a deeper understanding of the electronic excitations observed in the experimental UV-vis spectra of C-1 and C-2 complexes. The B3LYP functional with a mixed basis set was used for the Cu(II) complexes, with the 6-31G (d, p) basis set applied to the H, C, N, F, Cl, and O atoms, and the LANL2DZ basis set used for the copper metal [30,32,33].

It is noteworthy that the electronic excitations for both C-1 and C-2 complexes exhibit a narrow range from 445 to 448 nm, as shown in Table S2. C-1 has an intense absorption at 445 nm. When chlorine atom is replaced with fluorine atom, the absorption energy red-shifts slightly, and C-2 has an intense absorption at 448 nm. In both complexes, the main transition is from HOMO to LUMO.

The decrease in HOMO and LUMO energies was observed after replacing chlorine with fluorine (Table S3). The HOMO and LUMO orbitals of the C-1 and C-2 complexes are spread out over the ligand and the copper ion. This suggests that charge is transferred from the ligand to the copper ion during the electronic transitions. The HOMO is primarily located on the ligand, while the LUMO is localized on the copper ion (Figure S6), indicating that the ligand donates electrons to the copper ion upon excitation.

The photoluminescence spectra of the Cu (II) complexes (C-1 and C-2) were measured in solid phase using a 2 nm slit. The complexes were excited at their respective maximum wavelengths, 550 nm for C-1 and 555 nm for C-2. The spectra showed that the rate of recombination of electron-hole pairs was low, [30] indicating that there was a potential for charge separation or charge trapping in the Cu (II) complexes [24]. The spectral emission was caused by the excited h<sup>+</sup> and e<sup>-</sup> recombination. A lower emission indicates a lower rate of charge carriers' recombination. The emission strength of C-2 was found to be six-fold lower than that of C-1, indicating that C-1 had a lower rate of recombination compared to C-2. The smaller emission energy of the C-1 complex suggests that it has a lower rate of recombination of charge carriers, as shown in Figure 8.

As shown in Figure 9, FESEM images were said to be the most important evidence after coordination for determining the shape of Cu (II) complexes. The consequence showed that there were ample Cu (II) complexes in nanostrips and nanoribbons with a smaller facet ratio, similar to dm (diameter) and flat surfaces. This was an imaginable spectacle in the solvo-thermal preparation of Cu (II) complex nanostrips and nanoribbons [25]. Figure 9 exhibits the morphology of reported complexes stimulated in ethanol solution. The outcome designated that Cu<sup>2+</sup> ions were successfully coordinated with ligands, and the morphology compared with ligands was entirely changed.

### 3.2. Photocatalysis

The photocatalytic activity of Cu (II) complexes is investigated by the photodegradation of methylene blue (MB) and methyl violet (MV) dyes below the visible-light treatment. The time-based change in MB [20] and MV [24] concentrations with treatment time in the blank (no catalyst) and existence of C-1/C-2 are revealed in Figure 10. As the irradiation time rises, MB and MV photodegrade more quickly. In the absence of a photocatalyst, MB and MV are observed to experience 2% photodegradation, which may be the result of photolysis. Under the same experimental circumstances, the photodegradation of MB dye is 5% and 2%, respectively, in the presence of simple ligands and blank [24]. However, after 30 min of exposure to visible light, the photodegradation of MB and MV dyes with



C-1 was approximately 56% and 72%, respectively. Similarly, with the C-2 complex, the photodegradation was approximately 97% (MB) and 99% (MV) after 30 min of visible-light irradiation. As a result, C-2 exhibits greater photocatalytic activity in the current study against MB and MV photodegradation compared to the C-1 complex.

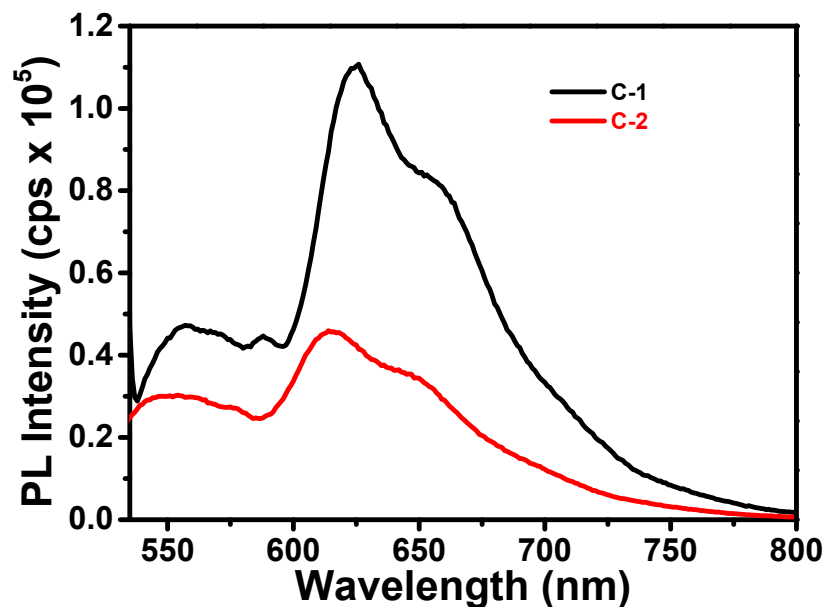


Figure 8. Photoluminescence spectra of C-1 and C-2 complexes.

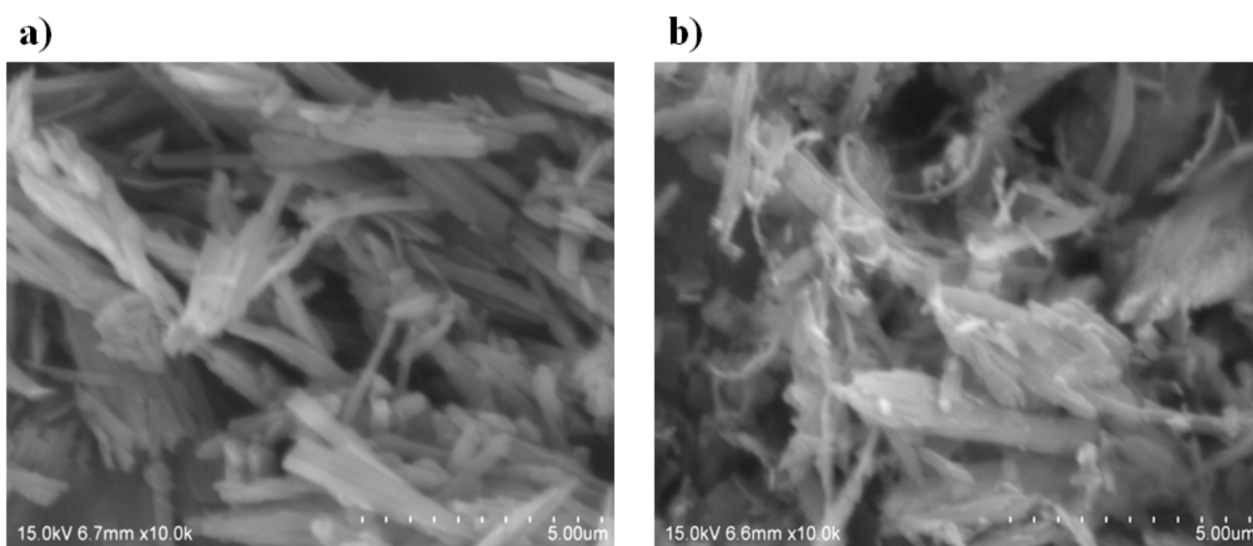


Figure 9. FESEM images of (a) C-1 and (b) C-2 complexes.

The photocatalytic decay of organic dye contaminants in the existence of Cu (II) complexes was initiated by the photogenerated electrons and holes, which ultimately produced free radicals such as  $\bullet\text{OH}$  and  $\text{O}_2\bullet$ . The photodegradation rate is straightly proportional to the possibility for the generation of these radicals on the photocatalyst surface and their reaction with the dye molecules [24]. The formation of hydroxyl radicals throughout the MB and MV photodegradation processes in the occurrence of Cu (II) complexes has been determined experimentally using benzoquinone (BQ) as a superoxide radical quencher [23,24,34,35]. Under equal conditions, photodegradation of MB or MV is carried out by adding 0.5 g of BQ in the presence of C-2. The photocatalytic activity of C-2 was inhibited for the first 5 min of irradiation with the addition of BQ. Even after 30 min of irradiation in presence of BQ, photodegradation of the MB dye was about 20%

(Figure 11a). As a result, in addition to  $O_2^\bullet$ , other active species such as holes were also involved in dye degradation. The possible MB and MV photodegradation processes using Cu (II) complexes as photocatalysts are shown in Figure 11b. The photocatalytic performance of the Cu (II) photocatalyst to photodegrade the organic dyes is directly related to the degree of generation of active  $O_2^\bullet$  radicals throughout the visible-light irradiation method [25]. Therefore, the greater photocatalytic activity of C-2 than C-1 can be attributed to observations in this study.

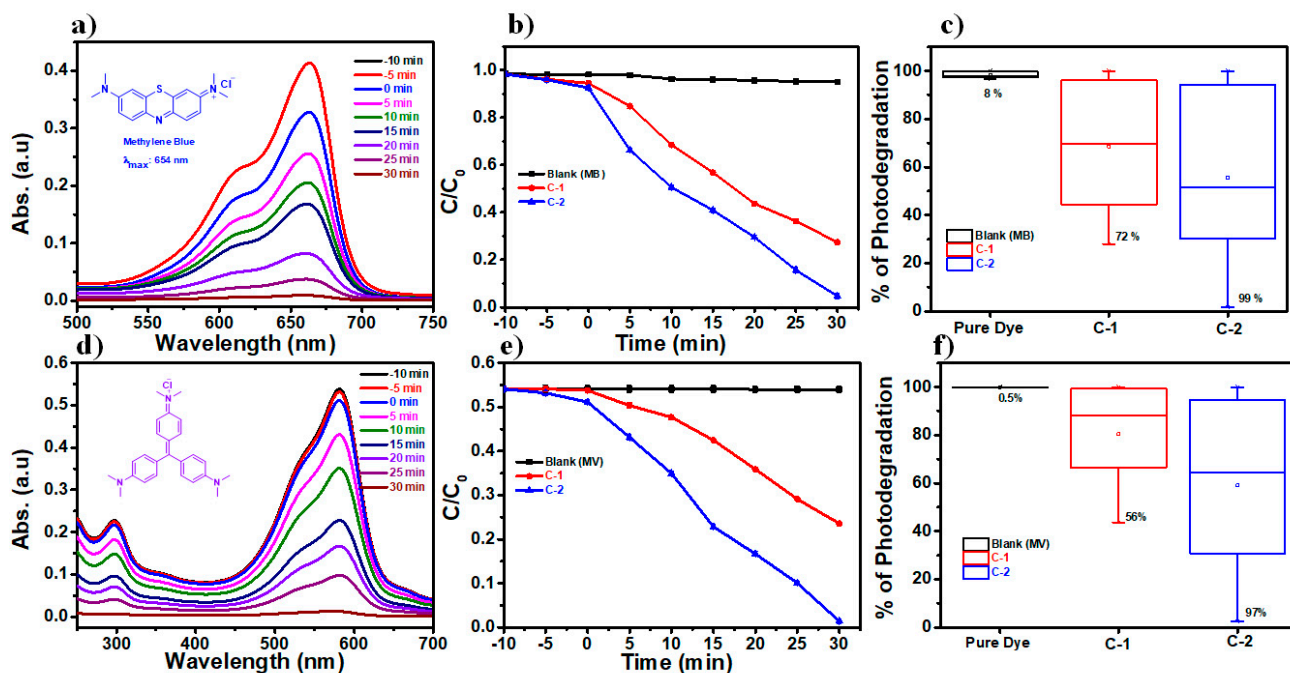


Figure 10. (a,d) Chronological absorbance curves; (b,e) photocatalytic plots, and (c,f) % photodegradation of MB and MV dyes in the presence of blank, C-1, and C-2 under visible-light irradiation.

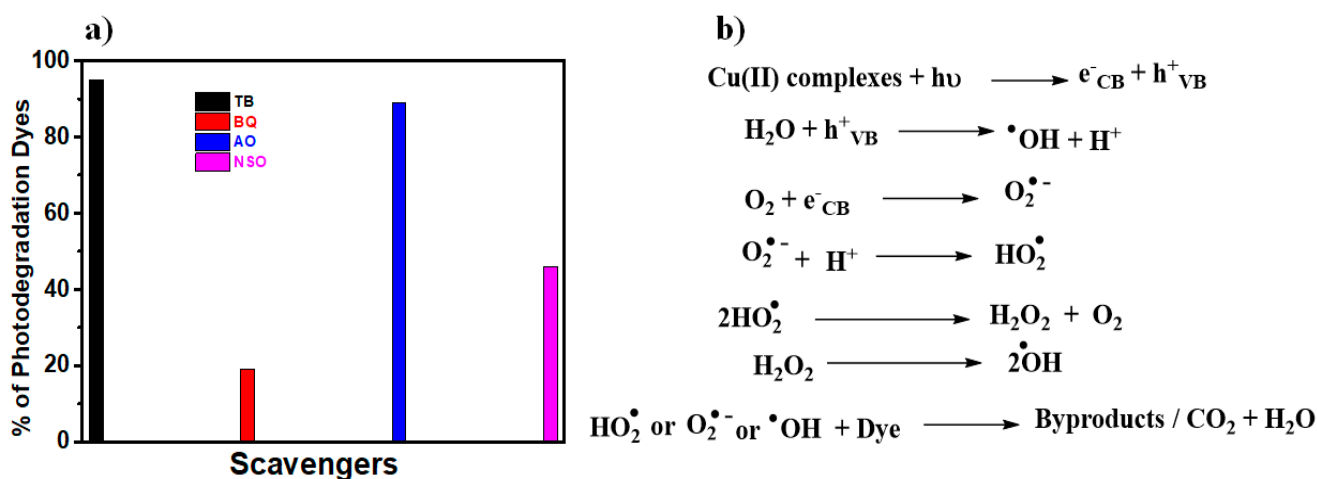


Figure 11. (a) Scavengers under visible-light irradiation and (b) Mechanistic studies in the presence of C-2 complex.

The kinetic curves of the C-2 photocatalytic reaction indicated that it had enhanced catalytic efficacy over C-1 and blank photocatalysts (Figure 12). The photoreaction kinetic graph was plotted against  $\ln(C/C_0)$  vs. time because of the photodegradation efficiency of MB and MV dye solutions, as shown in Figure 12a,b, and followed the pseudo-first order rate constant (Equation (1)). The rate constant ( $k$ ) of photodegradation of MB dye was 4.4 and 158.4  $\text{min}^{-1}$ , which is more than 35 times higher for C-2 as compared with

C-1 complex [24]. Similarly, the  $k$  value of photodegradation for MV dye was 2.3 and  $201.2 \text{ min}^{-1}$ , which is more than 87 times higher for C-2 as compared with C-1 complex [24].

$$\ln(C_0/C) = kt \quad (1)$$

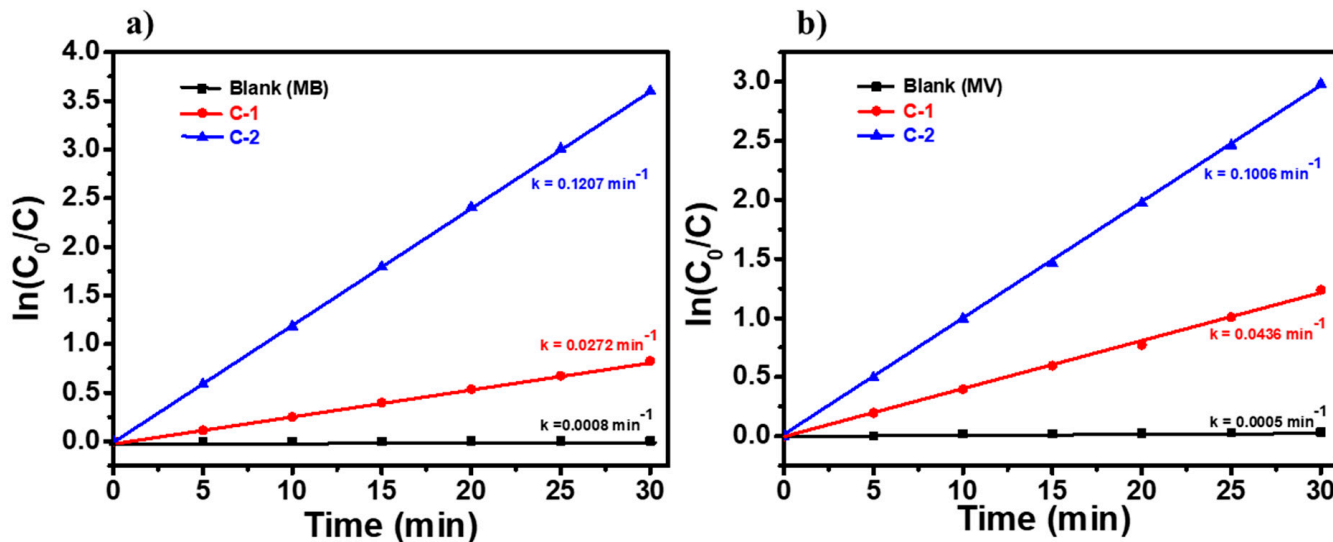


Figure 12. Kinetic plots for (a) MB and (b) MV dye solution in the presence of C-1 and C-2 complexes under visible-light irradiation.

The results from the transient photocurrent measurement suggest that the C-2 complex has a higher charge-species separation and relocation efficiency than the C-1 complex under visible-light irradiation (Figure 13a). The high transient photocurrent response of C-2 indicates that the complex can generate and separate charge carriers effectively. In contrast, C-1 showed a lower transient photocurrent response and a quicker decay, which suggests a greater recombination rate for the charge carriers. These results suggest that C-2 can utilize visible light more efficiently than C-1 to generate and separate charge carriers, leading to a higher photocurrent response. Overall, the transient photocurrent measurement provides valuable insights into the charge separation and recombination dynamics of the Cu-complexes under visible-light irradiation [24].

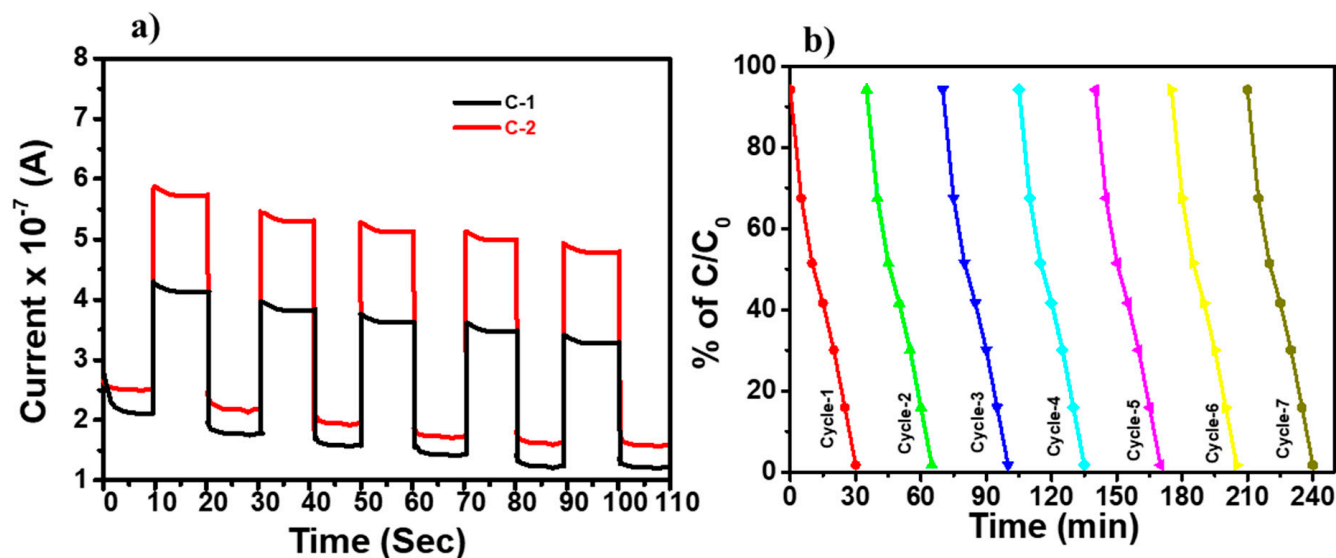
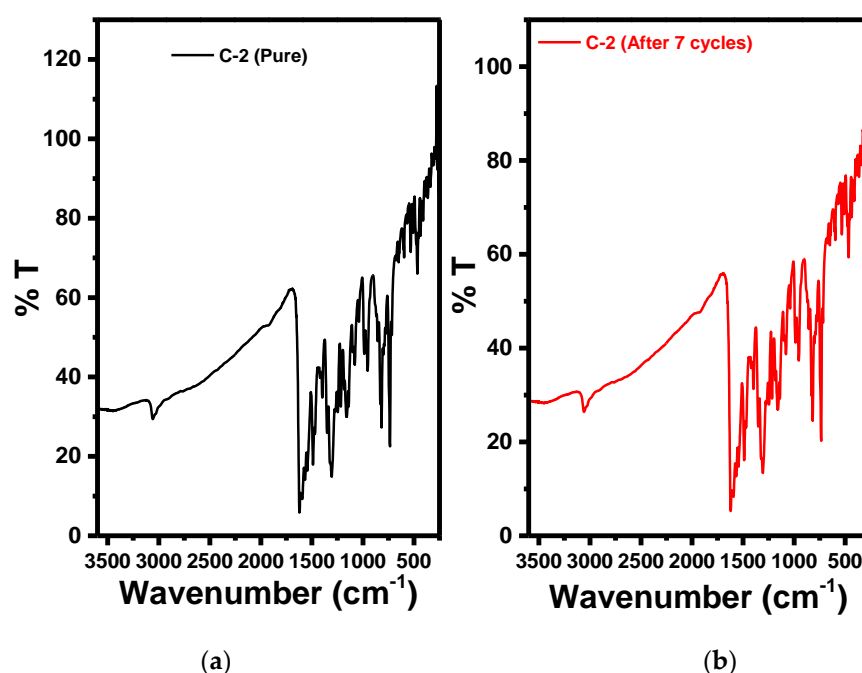


Figure 13. (a) The photocurrent response of C-1 and C-2 complexes and (b) recycling tests of C-2 complex for MB dye photodegradation.

Seven cycles of photocatalytic degradation were utilized to study the reusable nature of the C-2 catalyst. The catalyst C-2 utilized in every cycle of the photodegradation reaction was separated and cleaned with double-distilled water, vacuum desiccated, and reprocessed in the succeeding sequence of the degradation reaction. As revealed in Figure 13b, the photocatalytic degradation amount of the MB dye solutions still accomplished 97% after seven sequences of photoreaction. It has been established that the C-2 catalyst has an outstanding reuse characteristic, to a certain point. After the seventh cycle of photocatalysis, the photocatalyst C-2 was collected, verified by FTIR, and compared with pure C-2 catalyst, as revealed in Figure 14 [23,24]. As a result, the C-2 complex is highly stable under photocatalysis.



**Figure 14.** FTIR spectra of the C-2 complex: (a) pure; (b) photocatalysis following seven cycles of the photodegradation process.

#### 4. Conclusions

In conclusion, the copper (II) complexes were effectively synthesized and characterized using a variety of different methodologies. Cationic dyes were used in the experiment to test the photocatalytic potential of the complexes by seeing how they were degraded in the light. According to the findings, the photocatalytic performance of the C-2 complex was superior to that of the C-1 complex. This superiority may be attributed to the C-2 complex's narrower bandgap energy, bigger surface area, lower rate of recombination of charge carriers, lower emission strength, and stronger photocurrent sensing. Based on these observations, it would seem that the C-2 complex has the potential to function as an efficient photocatalyst in the process of degrading organic dye pollutants.

**Supplementary Materials:** The following supporting information can be downloaded at: <https://www.mdpi.com/article/10.3390/photochem3020016/s1>, Table S1: Physicochemical and elemental data of C-1 and C-2 complexes; Table S2: Electronic excitations ( $\lambda_{CAL}$  in nm), oscillator strength ( $f$ ), major transitions (MT), and % weight (%Ci) of C-1 and C-2 complexes by using TD-B3LYP/6-31G (d, p) method; Table S3: Calculated HOMO and LUMO energies, and HLG (in eV) for the Cu (II) complexes; Figure S1: HR MALDI mass spectrum of the C-1 complex; Figure S2: HR MALDI mass spectrum of the C-2 complex; Figure S3: Powder XRD image of CuO residue obtained from TG analysis; Figure S4: FTIR spectra of the L-1 ligand (a,c) and C-1 complex (b,d); Figure S5: FTIR spectra of L-2 ligand (a,c) and C-2 complex (b,d); Figure S6: Frontier molecular orbitals of the C-1 and C-2 complexes.

**Author Contributions:** Conceptualization, S.P. and P.C.; methodology, R.V.; software, P.C.; validation, S.P. and P.C.; formal analysis, R.K., R.P., M.S., R.G., M.R. and V.K.; investigation, M.S.; resources, S.P.; data curation, S.P.; writing—original draft preparation, M.S.; writing—review and editing, S.P. and P.C.; visualization, P.C.; supervision, S.P. and P.C.; project administration, S.P. and P.C.; funding acquisition, S.P. and P.C. All authors have read and agreed to the published version of the manuscript.

**Funding:** This research was funded by SERB (EMR//2014/000452), UGC-UPE-FAR and DST-PURSE, New Delhi, India, and CSIR (02(0339)/18/EMR-II), New Delhi, India.

**Data Availability Statement:** All the data related to this article is provided in the Supplemental Materials.

**Acknowledgments:** Authors especially thank DST-FIST schemes and UGC, New Delhi. Rohini Vallaboju thanks the DST-PURSE-II program, New Delhi, for its support.

**Conflicts of Interest:** The authors declare no conflict of interest.

## References

1. Mehmet, T. Polydentate Schiff-base ligands and their Cd(II) and Cu(II) metal complexes: Synthesis, characterization, biological activity and electrochemical properties. *J. Coord. Chem.* **2007**, *60*, 2051–2065.
2. Tunde, L.Y.; Segun, D.O.; Sizwe, Z.; Hezekiel, M.K.; Isiaka, A.L.; Monsurat, M.L.; Nonhlangabezo, M. Design of New Schiff-Base Copper(II) Complexes: Synthesis, Crystal Structures, DFT Study, and Binding Potency toward Cytochrome P450 3A4. *ACS Omega* **2021**, *6*, 13704–13718.
3. Liu, X.; Manzur, C.; Novoa, N.; Celedón, S.; Carrillo, D.; Hamon, J.-R. Multidentate unsymmetrically-substituted Schiff bases and their metal complexes: Synthesis, functional materials properties, and applications to catalysis. *Coord. Chem. Rev.* **2018**, *357*, 144–172. [[CrossRef](#)]
4. Wesley, J.A.; Kalidasa, M.K.; Neelakantan, M.A. Review on Schiff bases and their metal complexes as organic photovoltaic materials. *Renew. Sustain. Energy Rev.* **2014**, *36*, 220–227. [[CrossRef](#)]
5. Alberto, A.-M.; Viviana, R.-M.; Farrah, C.-B.; Jesús, R.P.-U.; Fernando, C.-C.; Dorian, P.-C.; Raúl, C.-P.; Galdina, V.S.-M.; Bethsy, A.A.-C.; David, M.-M. Pincer Complexes Derived from Tridentate Schiff Bases for Their Use as Antimicrobial Metallopharmaceuticals. *Inorganics* **2022**, *10*, 134.
6. Andreas, W.; Ulrich, S.S. Metal-Terpyridine Complexes in Catalytic Application—A Spotlight on the Last Decade. *ChemCatChem* **2020**, *12*, 2890–2941.
7. Takuya, S.; Ken-ichi, F. Recent Advances in Homogeneous Catalysis via Metal–Ligand Cooperation Involving Aromatization and Dearomatization. *Catalysts* **2020**, *10*, 635.
8. Kazimer, L.S.; Travis, R.B.; Tehshik, P.Y. Dual Catalysis Strategies in Photochemical Synthesis. *Chem. Rev.* **2016**, *116*, 10035–10074.
9. Manas, S.; Tannistha, R.B.; Armando, J.L.P.; Luísa, M.D.R.S.M. Aroylhydrazone Schiff Base Derived Cu(II) and V(V) Complexes: Efficient Catalysts towards Neat Microwave-Assisted Oxidation of Alcohols. *Int. J. Mol. Sci.* **2020**, *21*, 2832.
10. Ebrahimipour, S.Y.; Maryam, M.; Masoud, T.M.; Jim, S.; Joel, T.M.; Iran, S. Synthesis and structure elucidation of novel salophen-based dioxo-uranium(VI) complexes: In-vitro and in-silico studies of their DNA/BSA-binding properties and anticancer activity. *Eur. J. Med. Chem.* **2017**, *140*, 172–186. [[CrossRef](#)]
11. Atkins, R.; Brewer, G.; Kokot, E.; Mockler, G.M.; Sinn, E. Copper (II) and nickel (II) complexes of unsymmetrical tetradentate Schiff base ligands. *Inorg. Chem.* **1985**, *24*, 127–134. [[CrossRef](#)]
12. Kushwah, N.P.; Pal, M.K.; Wadawale, A.P.; Jain, V.K. Diorgano-gallium and-indium complexes with salophen ligands: Synthesis, characterization, crystal structure and C–C coupling reactions. *J. Organomet. Chem.* **2009**, *694*, 2375–2379. [[CrossRef](#)]
13. Santarupa, T.; Partha, R.; Ray, J.B.; Fallah, M.S.E.; Javier, T.; Eugenio, G.; Samiran, M. Ferromagnetic Coupling in a New Copper(II) Schiff Base Complex with Cubane Core: Structure, Magnetic Properties, DFT Study and Catalytic Activity. *Eur. J. Inorg. Chem.* **2009**, *2009*, 4385–4395.
14. Rong, M.; Wang, J.; Shen, Y.; Han, J. Catalytic oxidation of alcohols by a novel manganese Schiff base ligand derived from salicylaldehyd and l-Phenylalanine in ionic liquids. *Catal. Commun.* **2012**, *20*, 51–53. [[CrossRef](#)]
15. Teerawat, K.; Duangdao, C.; Bussaba, P.; Ratanon, C. Degradation of Methylene Blue with a Cu(II)–Quinoline Complex Immobilized on the Silica Support as a Photo-Fenton-Like Catalyst. *ACS Omega* **2022**, *7*, 33258–33265.
16. Soroceanu, A.; Cazacu, M.; Shova, S.; Turta, C.; Kožiček, J.; Gall, M.; Breza, M.; Rapta, P.; MacLeod, T.C.; Pombeiro, A.J. Copper (II) complexes with Schiff bases containing a disiloxane unit: Synthesis, structure, bonding features and catalytic activity for aerobic oxidation of benzyl alcohol. *Eur. J. Inorg. Chem.* **2013**, *2013*, 1458–1474. [[CrossRef](#)]
17. Ran, J.; Li, X.; Zhao, Q.; Qu, Z.; Li, H.; Shi, Y.; Chen, G. Synthesis, structures and photocatalytic properties of a mononuclear copper complex with pyridine-carboxylato ligands. *Inorg. Chem. Commun.* **2010**, *13*, 526–528. [[CrossRef](#)]
18. Mahesh, S.; Ramesh, G.; Venkanna, G.; Prabhakar, C.; Koteswar, R.R.; Someshwar, P. Effective photodegradation of organic pollutants in the presence of mono and bi-metallic complexes under visible-light irradiation. *J. Photochem. Photobiol. A Chem.* **2021**, *406*, 112996.
19. Venkanna, G.; Jakeer, A.; Mahesh, S.; Bhongiri, Y.; Ritu, M.; Chetti, P.; Someshwar, P. Evolution of physical and photocatalytic properties of new Zn(II) and Ru(II) complexes. *Polyhedron* **2019**, *170*, 412–423.

20. Someshwar, P.; Mahesh, S.; Ravinder, G.; Vithal, M.; Yu, T.T. New photocatalyst for allylic aliphatic C–H bond activation and degradation of organic pollutants: Schiff base Ti(IV) complexes. *RSC Adv.* **2015**, *5*, 58504–58513.
21. Guguloth, V.; Ahemed, J.; Subburu, M.; Guguloth, V.C.; Chetti, P.; Pola, S. A very fast photodegradation of dyes in the presence of new Schiff's base N<sub>4</sub>-macrocyclic Ag-doped Pd (II) complexes under visible-light irradiation. *J. Photochem. Photobiol. A Chem.* **2019**, *382*, 111975. [[CrossRef](#)]
22. Mahesh, S.; Ramesh, G.; Prabhakar, C.; Someshwar, P. Photooxidation of 2,2'-(Ethyne-1,2-diyl)dianilines: An Enhanced Photocatalytic Properties of New Salophen-Based Zn(II) Complexes. *Photochem* **2022**, *2*, 358–375.
23. Jakeer, A.; Jakeer, P.; Venkateshwar, R.D.; Ranjith, K.; Ramesh, G.; Yadagiri, B.; Prabhakar, C.; Someshwar, P. Synthesis of new Zn (II) complexes for photo decomposition of organic dye pollutants, industrial wastewater and photo-oxidation of methyl arenes under visible-light. *J. Photochem. Photobiol. A Chem.* **2021**, *419*, 113455.
24. Venkateshwar, R.D.; Mahesh, S.; Ramesh, G.; Manohar, B.; Prabhakar, C.; Babu, N.S.; Penumaka, N.; Yadagiri, B.; Someshwar, P. A new Zn(II) complex-composite material: Piezoenhanced photomineralization of organic pollutants and wastewater from the lubricant industry. *Environ. Sci. Water Res. Technol.* **2021**, *7*, 1737–1747.
25. Rohini, V.; Ranjith, K.; Radhika, P.; Mahesh, S.; Ramesh, G.; Manohar, B.; Someshwar, P.; Prabhakar, C. Enhanced piezo-photocatalytic properties of new salophen based Ti (IV) complexes. *Inorg. Chem. Commun.* **2023**, *148*, 110272.
26. Reddy, G.R.; Balasubramanian, S.; Chennakesavulu, K. Zeolite encapsulated Ni(ii) and Cu(ii) complexes with tetradentate N<sub>2</sub>O<sub>2</sub> Schiff base ligand: Catalytic activity towards oxidation of benzhydrol and degradation of rhodamine-B. *J. Mater. Chem. A* **2014**, *2*, 15598–15610. [[CrossRef](#)]
27. Hafsa, S.; Qureshi Fozia, M.S.; Haque, Z. Biosynthesis of Flower-Shaped CuO Nanostructures and Their Photocatalytic and Antibacterial Activities. *Nano-Micro Lett.* **2020**, *12*, 29.
28. Jiang, D.; Jianbin, X.; Liqiong, W.; Wei, Z.; Yuegang, Z.; Xinheng, L. Photocatalytic performance enhancement of CuO/Cu<sub>2</sub>O heterostructures for photodegradation of organic dyes: Effects of CuO morphology. *Appl. Catal. B Environ.* **2017**, *211*, 199–204. [[CrossRef](#)]
29. Janusz, G.; Katarzyna, Ś.; Julia, K.; Maciej, W. Multinuclear Ni(ii) and Cu(ii) complexes of a meso 6 + 6 macrocyclic amine derived from trans-1,2-diaminocyclopentane and 2,6-diformylpyridine. *Dalton Trans.* **2022**, *51*, 9735–9747.
30. Gülnur, K.K. Synthesis of new Schiff base and its Ni(II), Cu(II), Zn(II) and Co(II) complexes; photophysical, fluorescence quenching and thermal studies. *J. Mol. Struct.* **2022**, *1256*, 132534.
31. Nooshin, K.; Alison, Z.; Sheida, E. Bioactive Ni(II), Cu(II) and Zn(II) complexes with an N<sub>3</sub> functionalized Schiff base ligand: Synthesis, structural elucidation, thermodynamic and DFT calculation studies. *Inorg. Chim. Acta* **2022**, *541*, 121083.
32. Rasha, M.K.; Ahmed, S.; Aly, H.A.; Mohamed, M.A.F.-A. Development of a novel and potential chemical sensor for colorimetric detection of Pd(II) or Cu(II) in E-wastes. *Microchem. J. Part A* **2022**, *172*, 106951.
33. Frisch, M.J.; Trucks, G.W.; Schlegel, H.B.; Scuseria, G.E.; Robb, M.A.; Cheeseman, J.R.; Scalmani, G.; Barone, V.; Petersson, G.A.; Nakatsuji, H.; et al. *Gaussian 16W, Revision B.01*; Gaussian, Inc.: Wallingford, CT, USA, 2016.
34. Minji, Y.; Youngtak, O.; Sugyeong, H.; June, S.L.; Ramireddy, B.; Sun, H.K.; Filipe, M.M.; Sang, O.K.; Dong, H.K. Synergistically enhanced photocatalytic activity of graphitic carbon nitride and WO<sub>3</sub> nanohybrids mediated by photo-Fenton reaction and H<sub>2</sub>O<sub>2</sub>. *Appl. Catal. B Environ.* **2017**, *206*, 263–270.
35. Jiahui, L.; Xinghui, L.; Yan, C.; Huijun, L.; Ruochang, L.; Xiaoli, D.; Hyoyoung, L.; Hongchao, M. Highly Enhanced Photoelectrocatalytic Oxidation via Cooperative Effect of Neighboring Two Different Metal Oxides for Water Purification. *J. Phys. Chem. C* **2020**, *124*, 11525–11535.

**Disclaimer/Publisher's Note:** The statements, opinions and data contained in all publications are solely those of the individual author(s) and contributor(s) and not of MDPI and/or the editor(s). MDPI and/or the editor(s) disclaim responsibility for any injury to people or property resulting from any ideas, methods, instructions or products referred to in the content.